

# First order phase transition from the vortex liquid to an amorphous solid

M. Menghini<sup>1</sup>, Yanina Fasano<sup>1</sup>, F. de la Cruz<sup>1</sup>, S.S. Banerjee<sup>2</sup>, Y. Myasoedov<sup>2</sup>, E. Zeldov<sup>2</sup>, C. J. van der Beek<sup>3</sup>, M. Konczykowski<sup>3</sup> and T. Tamegai<sup>4</sup>

<sup>1</sup>*Instituto Balseiro and Centro Atómico Bariloche, CNEA, Bariloche, 8400, Argentina*

<sup>2</sup>*Department of Condensed Matter Physics, Weizmann Institute of Science, Rehovot 76100, Israel*

<sup>3</sup>*Laboratoire des Solides Irradiés, CNRS UMR 7642, Ecole Polytechnique, 91128 Palaiseau, France*

<sup>4</sup>*Department of Applied Physics, The University of Tokyo, Hongo, Bunkyo-ku, Tokyo 113-8656, and CREST Japan Science and Technology Corporation (JST), Japan*

(February 1, 2008)

We present a systematic study of the topology of the vortex solid phase in superconducting  $\text{Bi}_2\text{Sr}_2\text{CaCu}_2\text{O}_8$  samples with low doses of columnar defects. A new state of vortex matter imposed by the presence of geometrical contours associated with the random distribution of columns is found. The results show that the first order liquid-solid transition in this vortex matter does not require a structural symmetry change.

As a consequence of the interaction between vortices and quenched disorder in superconducting samples, the vortex liquid solidifies through a first order phase transition (FOT) [1–3] into a topologically ordered solid with elastic deformations, the Bragg glass phase [4,5]. Artificially introduced correlated defects, as those produced by heavy ion irradiation, transform the first order liquid-solid transition into a second order one in which the solid vortex phase, the Bose Glass [6], has no topological quasi long range order. However, studies [7] of the phase diagram of  $\text{Bi}_2\text{Sr}_2\text{CaCu}_2\text{O}_8$  (BSCCO-2212) have shown that the FOT is robust in the presence of low density of columnar defects. In this case the FOT is preserved even for vortex densities comparable to those of defects.

High dose of columnar defects has two main effects on the vortex system. On one hand, its random distribution suppresses the FOT; on the other hand, the correlated potential hardens the vortex lines inducing a divergent vortex tilting elastic constant,  $C_{44}$ , at the Bose Glass transition. The results in Ref. [7] indicate that the disorder induced by a low density of columnar defects is too weak to change the order of the liquid-solid transition. This could imply that the quasi long range order of the Bragg Glass is preserved despite the presence of correlated defects.

The aim of this work is to establish the correlation between the space configuration of columnar defects and the vortex structure created in the presence of those defects. This goal is achieved visualizing the vortex structure by means of the magnetic decoration technique in samples where the liquid-solid phase transition has been characterized by differential magneto optics (DMO) [8]. The observed vortex topology is discussed in terms of the nature of the liquid-solid transition.

The BSCCO-2212 samples used in this work were irradiated at GANIL by 1 GeV Pb ions parallel to the  $c$  axis of the crystal. In order to compare the vortex structure in the presence of columnar defects with that

of the pristine sample, the irradiation was made through an ad-hoc stainless steel mask that allows to have irradiated and non irradiated regions in the same sample (see inset of Fig 1(a)). We have investigated four samples irradiated with doses corresponding to  $B_\Phi = 5, 10, 50$  and 100 G, where  $B_\Phi$ , the matching field, is usually defined as  $n_{col}\Phi_0$  with  $n_{col}$  the density of columns and  $\Phi_0$  the flux quantum. The  $H - T$  phase diagram obtained by DMO imaging [9] for these samples is shown in Fig. 1(a). It is important to remark that this high sensitivity technique shows that the FOT is not only preserved in the presence of low density of columnar defects but the transition temperature is raised when compared to that of pristine samples. For samples with  $B_\Phi = 5$  and 10 G the melting line is first order and for the  $B_\Phi = 100$  G sample is continuous in the range of fields investigated by magnetic decoration. For the  $B_\Phi = 50$  G sample a critical point at 70 G separating the FOT at lower fields from a continuous one at higher fields is found. The magnetic decoration was performed after cooling the sample in the presence of a field, FC experiment, down to 4.1 K. The results obtained in the non irradiated regions confirm the high quality of the crystals.

Figure 1(b) shows the vortex structure in the non irradiated and irradiated regions obtained by magnetic decoration after FC the  $B_\Phi = 10$  G sample in a field of 40 G. A sharp boundary separates the Bragg Glass in the non irradiated region from a structure with no long range crystalline order in the irradiated one.

The experimental results show that the vortex structure is polycrystalline for  $B > B_\Phi$  and amorphous in the range  $B < B_\Phi$ . Examples of Delaunay triangulations of polycrystalline vortex structures observed by magnetic decoration after FC the  $B_\Phi = 10$  G sample in fields of 80 G and 40 G are shown in Fig. 2(a) and (b), respectively. Fig. 2(c) shows the vortex structure for  $B = B_\Phi$ . The black dots indicate topological defects (non-sixfold coordinated vortices). Figure 3 depicts decoration images

of amorphous structures obtained in the regime  $B < B_\Phi$ ;  
 (a) after FC the  $B_\Phi = 50$  G sample in a field of 30 G and  
 (b) after FC the  $B_\Phi = 100$  G sample in a field of 80 G.

Contrary to what is often observed in homogeneous materials, we argue that the nature of the polycrystalline structure shown in Fig. 2 is an intrinsic property of the vortex matter in the presence of randomly distributed correlated defects. To demonstrate this we have used the dynamic annealing method [10,11] in which the magnetic field is tilted back and forth before the decoration is made. This procedure is known to remove the grain boundaries in  $\text{NbSe}_2$  and to reorder the crystalline vortex lattice [10] in non irradiated BSCCO-2212 samples. In contrast, we find that the polycrystalline structure of the irradiated region is not altered after applying this annealing procedure. This supports that the observed structure is the equilibrium one rather than a metastable configuration resulting from the typical nucleation and growth processes.

The above discussion suggests that the grain boundaries of the polycrystalline structure are fixed in space by the random distribution of columnar defects. If this were the case the area of the grains for a given  $B_\Phi$  would be field independent contrary to what is observed in homogeneous low  $T_c$  superconductors. To verify this, we studied the statistical distribution of the grain areas as a function of the applied field for  $B_\Phi = 5$  and 10 G samples. The grain boundaries are defined as the interface between crystallites which orientations differ by 10 degrees or more. The areas of the different grains are measured counting the number of vortices within them. The analysis of many pictures shows that the histogram of the grain sizes is broad with upper and lower limiting values for the grain areas for each applied field. The number of vortices,  $N_{vg}$ , within the largest and smallest grains (upper and lower limits of the histogram) are proportional to  $B$  as shown in Fig. 4 for  $B_\Phi = 10$  G sample. Identical behavior is found in the  $B_\Phi = 5$  G sample with the shift of the distribution of grain areas corresponding to the lower irradiation dose. Furthermore, the average number of vortices per grain (defined as the ratio between the total number of vortices within grains and the number of grains) is also found to be proportional to  $B$ , see Fig. 4 (solid squares). These results make evident that the size of the different grains for a given  $B_\Phi$  is field independent contrary to what is found in low  $T_c$  superconductors, where the average grain size grows with the magnetic field [12]. The invariance of the grain size with  $B$  in the irradiated regions strongly supports that the grain size as well as the space distribution of the grains are determined by the landscape of the columnar defects.

In order to understand the relation between grain boundaries and the distribution of correlated defects we have generated a set of random points simulating the positions of columnar defects, see Fig. 2(d) (white dots). This configuration is found to be equivalent to that of

columnar defects detected after etching mica irradiated by heavy ions with comparable doses, see inset in Fig. 4. It is interesting to remark that the distribution of columnar defects is not homogeneous on the scale of the lattice parameter in the range of fields investigated. The in-plane inhomogeneous distribution and the correlated character of the columnar defects suggest the presence of a network of contours extending throughout the thickness of the sample associated with the localization of vortices on columns. In Fig. 2(d) the contours are represented by the gray connected areas indicating the range of interaction (penetration depth) of vortices localized on defects. These vortices create energy barriers that inhibit the propagation of the crystalline vortex lattice, giving rise to the polycrystalline structure observed in the regime  $B > B_\Phi$ . Thus, the observed grain boundaries in samples with low irradiation dose have a different origin than those associated with metaestable states in homogeneous systems [11]. The apparent grain boundaries in the irradiated samples are field independent vortex contours fixed in space by the random distribution of columns. This prompts us to propose a new state of vortex matter where the total number of vortices is divided in two species, one corresponds to the fraction of vortices localized on contours,  $\rho_{cont}$ , and the other forming the crystallites surrounded by the contours,  $\rho_{crys}$ .

Based on the above discussion we present a simplified picture that allows to predict the dependence of the number of topological defects (non sixfold coordinated vortices) of the polycrystalline structure,  $N_{def}$ , on  $B$  and  $B_\Phi$ . The total number of defects is counted in an arbitrary large area that contains many grains. The reported data was obtained from an inspected area of the order of  $10^4 \mu\text{m}^2$ , much larger than the maximum grain size for the different  $B_\Phi$  investigated. From the inspection of many images of the vortex structure in the irradiated regions we find that most of the topological defects are located along the contours separating the crystallites. Thus, as a first order approximation we assume that  $N_{def}$  is proportional to the number of vortices localized on the contours,  $N_{cont}$ . The total length of the contours within the inspected area can be written as  $L = N_{cont} a_0$  where  $a_0$  is the average vortex distance. The experimental results showing the field independence of the areas of the crystallites (see Fig. 4) imply that  $L$  is only function of  $B_\Phi$ . Therefore  $N_{def} \propto N_{cont} \propto L(B_\Phi)/a_0 \propto L(B_\Phi)B^{1/2}$ . On the other hand, the self similarity of the space distribution of random columnar defects imposes that the areas enclosed by the contours scale with  $B_\Phi$  and consequently  $L(B_\Phi) \propto B_\Phi^{1/2}$ . Therefore, the fraction of vortices involved in topological defects,  $\rho_{def}$ , is

$$\rho_{def} = N_{def}/N_v \propto (B_\Phi/B)^{1/2} \quad (1)$$

In Fig. 5 we plot  $\rho_{def}$  obtained from Delaunay triangu-

lations of vortex structures for all  $B$  and  $B_\Phi$  investigated. The black line corresponds to the square root dependence predicted by Eq. 1. Despite the crude approximations,  $N_{def} \propto N_{cont}$  and  $L(B_\Phi) \propto B_\Phi^{1/2}$ , we see that for  $B_\Phi < B$  the experimental results are well described by this simple model. On the other hand, the deviation of the experimental data from the dependence predicted for  $\rho_{def}$  in the range  $B_\Phi/B > 1$  is evident.

The failure of the model to describe the amorphous state is expected, since for fields  $B \leq B_\Phi$  a significative fraction of the areas enclosed by the contours fixed in space are not large enough to allocate vortices with crystalline symmetry,  $\rho_{crys} \approx 0$ . In this limit, despite most of the vortices remain pinned on columns,  $\rho_{cont} \approx 1$ , the number of topological defects is not proportional to  $L(B_\Phi)/a_0$ ; i.e.  $a_0$  is not an appropriate length scale to apply the scaling argument.

The  $B_\Phi/B$  independence of the fraction of defects in the amorphous state ( $\rho_{def} \approx 0.5$ ) is remarkable, see Fig. 5. To investigate the origin of this result we have generated a random distribution of points with the constrain that the distance between near neighbors is not less than 50% of the lattice parameter of a perfect lattice with the same density. The constrain is chosen to allow the fluctuations of the average distance between points to be that observed in the amorphous vortex structure. It is found that the fraction of defects obtained from Delaunay triangulation of this simulated distribution of points is the same as that for the vortex structure for  $B < B_\Phi$ , indicating that in this regime most of the vortices are pinned on a random distribution of columnar defects.

The analysis of the vortex structure for  $B > B_\Phi$  as well as for  $B < B_\Phi$ , Fig. 5, strongly supports that in both limits the topological defects are associated with vortices localized on columns. For  $B > B_\Phi$  the topological defects of the vortex structure are mainly due to plastic distortions induced by the presence of crystallites. In the other limit,  $B < B_\Phi$ , the space within the contours does not allow to form crystallites,  $\rho_{crys} \approx 0$ , and the defects are associated with vortices localized on a fraction of columns compatible with the constrain mentioned above. It is clear that  $B/B_\Phi \approx 1$  marks the transition from a topological state described by a collection of crystallites to a state characterized by an amorphous structure, both determined by the random distribution of columns.

As a consequence of the results discussed above we see that in the limit  $B < B_\Phi$  no crystalline structure can be accommodated within the small contours determined by the columnar defects,  $\rho_{crys} \approx 0$ . Thus, an amorphous vortex structure characterizes the solid state. This is particularly relevant when analyzing the interrelation between the solid structure and the nature of the vortex liquid-solid transition. The critical point at 70 G in the phase diagram of the  $B_\Phi = 50$  G sample indicates that most of the field range where the first order melting

takes place corresponds to the regime  $B < B_\Phi$ . Thus, the observed amorphous vortex structure, see Fig. 3(a), rules out the widely accepted correlation between a first order liquid-solid transition and a structural symmetry transformation. Moreover, we observe no difference between the topological order in Figs. 3 (a) and (b) despite the fact that the former structure has solidified through a FOT whereas the latter through a continuous phase transition.

In summary, a new vortex matter with two types of vortices has been discovered, giving support to the recently suggested vortex porous structure [9] and the interstitial liquid [13]. One type is associated with vortices localized upon the topological contours formed by the random distribution of columnar defects and the other with vortices forming the crystallites. The relative distribution of vortices in these two classes explains the topological transformation of the solid from a Bragg Glass ( $B_\Phi = 0$ ) into a polycrystal ( $B_\Phi < B$ ) and then into an amorphous structure ( $B_\Phi > B$ ) as the density of columnar defects is increased. The lack of correlation between the structure of the vortex solid and the order of the melting transition opens an important question on the microscopic mechanism that triggers melting in vortex solids. The detection of a FOT between an amorphous solid and a liquid makes evident that the first order melting transition in vortex matter does not require the widely accepted long range structural order of the solid state.

MM, YF and FC acknowledge E. Jagla, P. Cornaglia and F. Laguna for useful discussions and suggestions. FC and EZ acknowledge the support by the Fundación Antorchas-WIS collaboration program. Work partially supported by ANPCYT PICT99-5117. M. M. and Y. F. hold a fellowship of CONICET.

---

- [1] H. Safar, P. L. Gammel, D. A. Huse, D. J. Bishop, J. P. Rice and D. M. Ginsberg, *Phys. Rev. Lett.* **69**, 824 (1992).
- [2] H. Pastoriza, M. F. Goffman, A. Arribere and F. de la Cruz, *Phys. Rev. Lett.* **72**, 2951 (1994).
- [3] E. Zeldov *et al.*, *Nature* **375**, 373 (1995).
- [4] T. Giamarchi and P. Le Doussal, *Phys. Rev. B* **52**, 1242 (1995).
- [5] T. Klein, I. Journaud, S. Blanchard, J. Marcus, R. Cubbit, T. Giamarchi and P. Le Doussal, *Nature* **413**, 404 (2001).
- [6] D. R. Nelson and V. M. Vinokur, *Phys. Rev. B* **48**, 13060 (1993).
- [7] B. Khaykovich, M. Konczykowski, K. Teitelbaum, E. Zeldov, H. Shtrikman and M. Rappaport, *Phys. Rev. B* **57**, R14088 (1998).

- [8] A. Soibel, E. Zeldov, M. Rappaport, Y. Myasoedov, T. Tamegai, S. Ooi, M. Konczykowski and V. Geshkenbein, *Nature* **406** 282 (2000).
- [9] S.S. Banerjee, A. Soibel, Y. Myasoedov, M. Rappaport, E. Zeldov, M. Menghini, Yanina Fasano, F. de la Cruz, C. J. van der Beek, M. Konczykowski and T. Tamegai, unpublished.
- [10] Yanina Fasano, M. Menghini, F. de la Cruz and G. Nieva, *Phys. Rev. B* **62**, 15183 (2000).
- [11] Yanina Fasano, M. Menghini, F. de la Cruz, Y. Paltiel, Y. Myasoedov, E. Zeldov, M. J. Higgins and S. Bhattacharya, *Phys. Rev. B* **66**, 020512(R) (2002).
- [12] M. V. Marchevsky Ph.D. Thesis, Kamerlingh Onnes Laboratory, Leiden University, Holland. 1996.
- [13] L. Radzihovsky, *Phys. Rev. Lett.* **74**, 4923 (1995).

FIG. 1. (a) Phase diagram obtained by DMO for the pristine BSCCO-2212 sample and for samples with columnar defect densities corresponding to  $B_\Phi = 5, 10, 50$  and  $100$  G. Solid lines indicate first order liquid-solid transition while dotted lines correspond to continuous ones. Inset: Schematics of the sample with the mask used for irradiation. (b) Magnetic decoration at  $40$  G in the sample with  $B_\Phi = 10$  G. The dashed line shows the boundary between the irradiated and the non-irradiated regions.

FIG. 2. Delaunay triangulations of the vortex structure in a sample with  $B_\Phi = 10$  G at fields of: (a)  $80$  G, (b)  $40$  G and (c)  $10$  G. The black dots indicate the non sixfold coordinated vortices. The gray lines in (a) and (b) depict the grain boundaries. (d) Set of random points (white dots) generated numerically simulating a distribution of columnar defects with  $B_\Phi = 10$  G. The gray areas indicate the range of interaction of vortices localized on defects, see text.

FIG. 3. (a) Structure of the vortex solid after a FOT at  $B = 30$  G in the  $B_\Phi = 50$  G sample. (b) Structure of the vortex solid after a continuous liquid-solid transition at  $80$  G in the  $B_\Phi = 100$  G sample.

FIG. 4. Number of vortices within the largest (triangles), the average (squares) and the smallest (circles) grains as a function of  $B$  for  $B_\Phi = 10$  G. Inset: Columnar defect distribution in mica irradiated with heavy ions.

FIG. 5. Fraction of defects,  $\rho_{def}$  as a function of  $B_\Phi/B$  for all  $B_\Phi$  investigated. The black line corresponds to  $\rho_{def} \propto (B_\Phi/B)^{1/2}$  and the gray dotted line to  $\rho_{def} = 0.5$ .

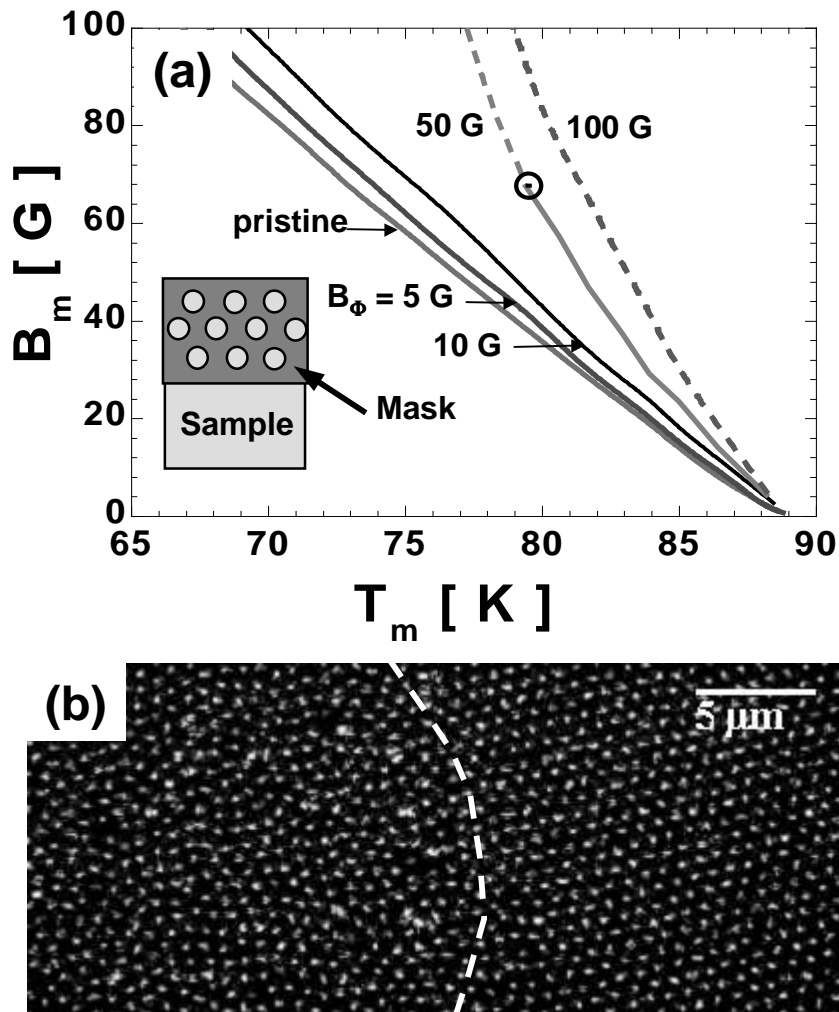
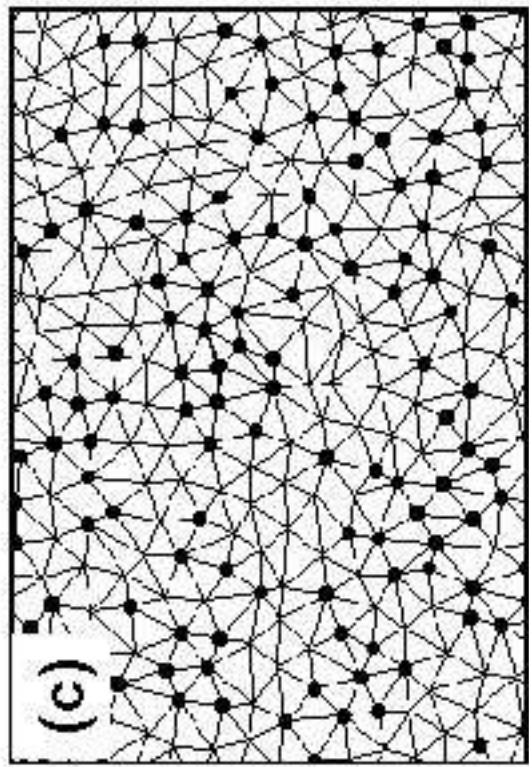
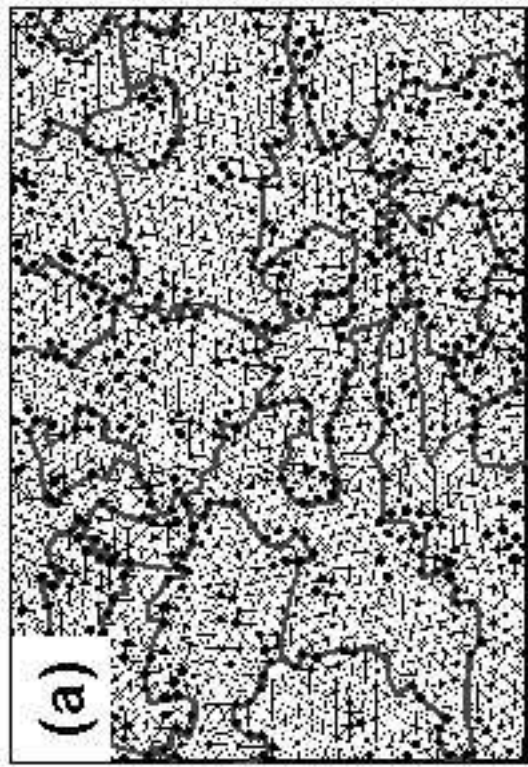
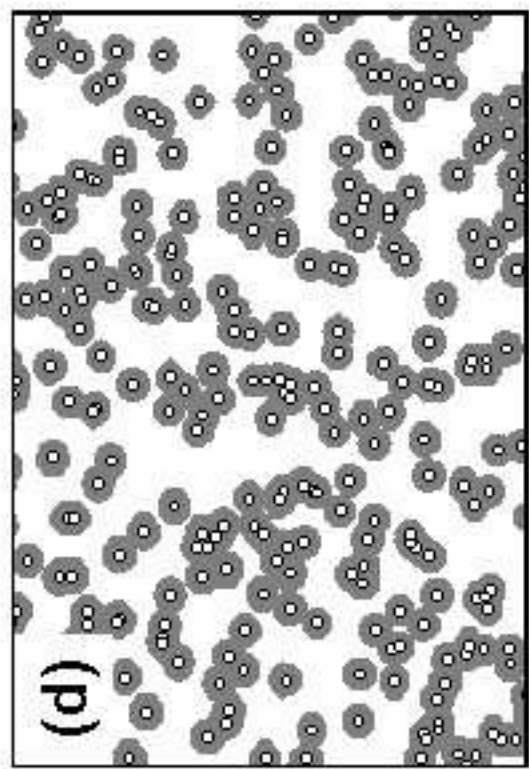
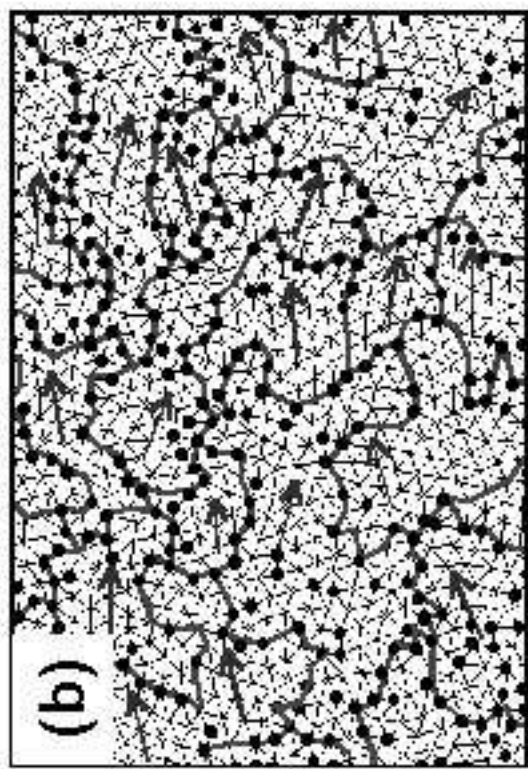


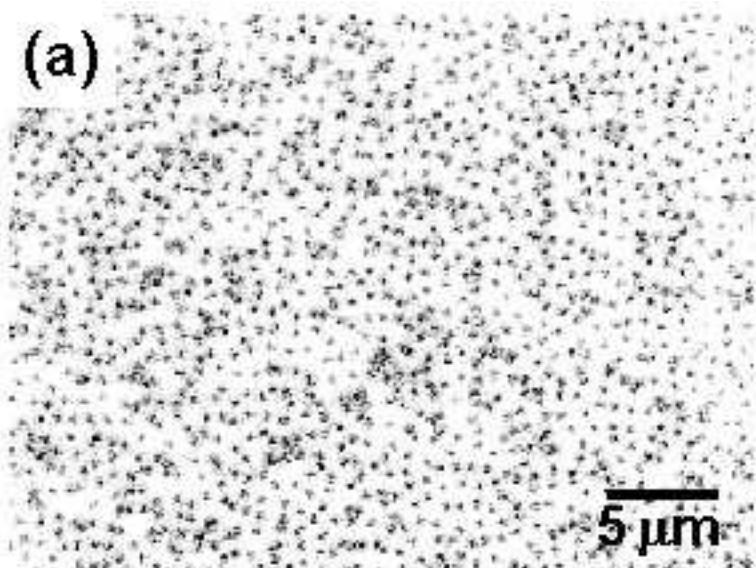
Figure 1, M. Menghini *et al.*

Figure 2, M. Menghini *et al.*



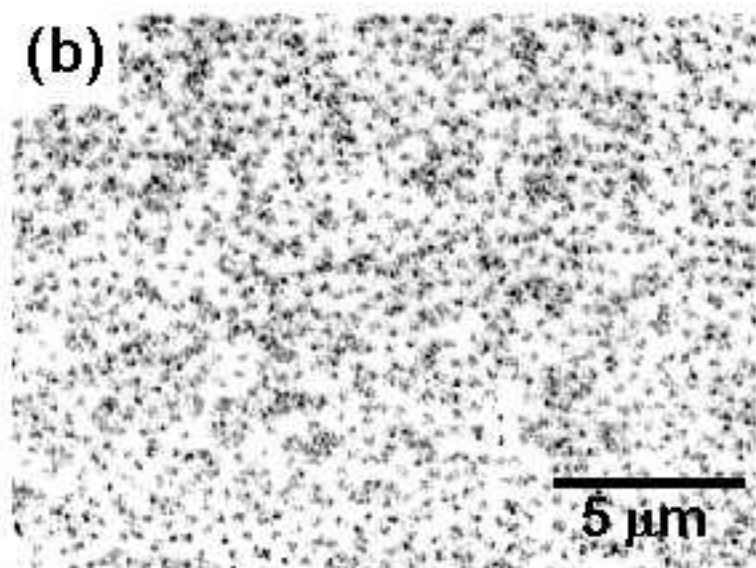
10  $\mu\text{m}$

(a)



5  $\mu\text{m}$

(b)



5  $\mu\text{m}$

Figure 3, M. Menghini *et al.*

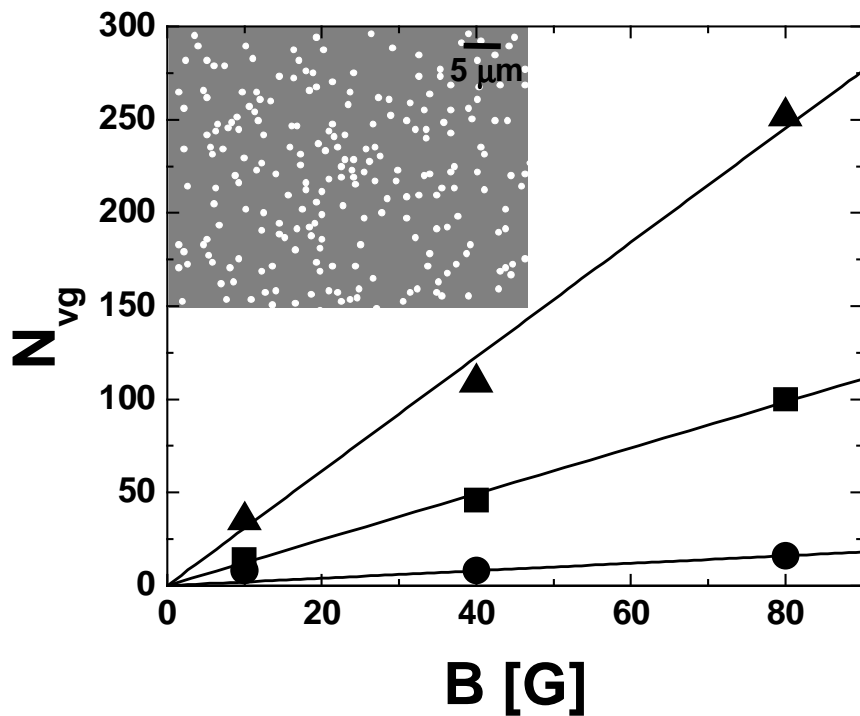


Figure 4, M. Menghini *et al.*

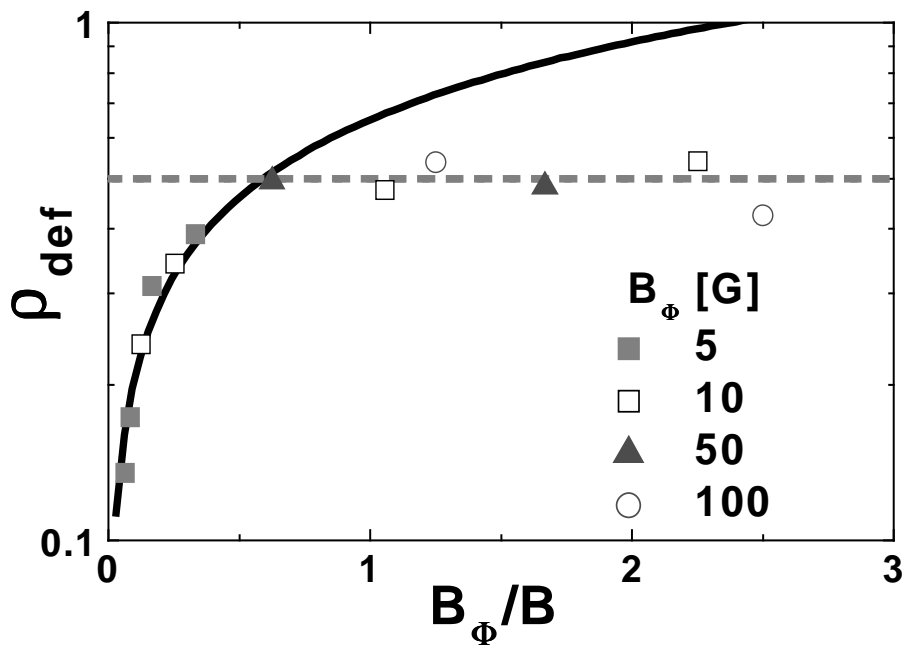


Figure 5, M. Menghini *et al.*